Molecular Dynamics Simulation of a Polymer Melt/Solid Interface: Local Dynamics and Chain Mobility in a Thin Film of Polyethylene Melt Adsorbed on Graphite

Vagelis A. Harmandaris, Kostas Ch. Daoulas, and Vlasis G. Mavrantzas*

Department of Chemical Engineering, University of Patras, GR 26504, Patras, Greece, and Institute of Chemical Engineering and High-Temperature Chemical Processes (FORTH-ICE/HT), GR 26504, Patras, Greece

Received January 27, 2005; Revised Manuscript Received April 8, 2005

ABSTRACT: Molecular dynamics (MD) simulations have been performed on a dense polymer melt adsorbed on a solid substrate on the one side and exposed to vacuum on the other. As a model system, a thin film of polyethylene (PE) melt supported by a crystalline graphite phase on its one side (the other surface of the film is free) has been examined. Most simulations have been carried out with unentangled PE melt systems, such as C_{78} and C_{156}, in the NPT statistical ensemble at $T = 450$ K and $P = 0$ atm for times up to 100 ns, using a multiple-time step MD algorithm and by incorporating the correct dependence of the long-range contribution to the energy and stress tensor on the density profile. To increase the statistical accuracy of the results, large systems have been employed in the MD simulations, such as a 200-chain C_{78} melt consisting of 15 600 carbon atoms. The MD simulation data have been analyzed to provide information about the spatial dependence of the short-time dynamical properties (conformational relaxation) of the melt and the long-time segmental motion and mobility in the film (transport and diffusion). Local mobility near the graphite phase is predicted to be highly anisotropic: although it remains practically unaltered in the directions x and y parallel to the surface, it is dramatically reduced in the direction z perpendicular to it. To calculate the long time self-diffusion coefficient of adsorbed segments in the direction perpendicular to the graphite plane, MD trajectories have been mapped onto the (numerical) solution of a macroscopic, continuum diffusion equation describing the temporal and spatial evolution of the concentration of adsorbed atoms in the polymer matrix. Our calculations prove that the diffusive motion of segments remains inhomogeneous along the z direction of the adsorbed film for distances up to approximately 5−6 times the root-mean-square of the radius of gyration, R_g, of the bulk, unconstrained melt.

I. Introduction

Polymer melt/solid and polymer melt/vacuum interfaces are encountered in many technologies involving adhesives, coatings, lubricants, and composite materials, where adsorbed molecules control the overall performance of the multiphase material system.[1−4] Today, such interfaces play a key role also in new applications involving hybrid materials where nanoparticles are added to polymer to alter its structural and mechanical properties without affecting the main chemical features of the supporting matrix.[5] Such nanocomposites exhibit dramatic changes in their glass transition temperature and dynamic mechanical properties as a function of filler volume fraction, thus opening up the way toward the design of new, nanostructured materials with enhanced mechanical, surface, and thermal characteristics.

In applications involving thin or ultrathin polymer films, in addition to the polymer/substrate interaction energy, knowledge of polymer mobility in the film (and how it is altered by the presence of the boundary) is absolutely necessary for controlling the wetting or friction properties of the interfacial system. This happens because chain mobility in the adsorbed film can have a strong influence on its rheological[5,6] and linear viscoelastic properties.[7,8] Developing simulation tools that establish a link between these properties and the chemical constitution of the material and its interatomic interactions is therefore highly desirable: through the construction of a hierarchy of tools that span all relevant length scales (from the atomistic to the mesoscopic to the macroscopic), one can understand structure−property−processing−performance relations in the composite or hybrid structure and then develop principles for optimal process and product design.

We recently[9] reported our findings from a computer simulation study that involves execution of preequilibration double-bridging Monte Carlo (DBMC)[10] runs of model PE melt films adsorbed on graphite on the one side and exposed to vacuum on the other, followed by production runs with a multiple-time step MD method. PE chains in the simulations were represented in atomistic detail as united atoms subject to bending, torsional, and (intra- and intermolecular) Lennard-Jones (LJ) interaction potentials. To calculate the potential energy of interaction between polymer atoms and the semiinfinite graphite substrate, the method designed by Steele,[11] and extensively used in the simulation studies of Mansfield and Theodorou,[12,13] and more recently of Daoulas et al.,[14,15] was implemented. The first part of this work[9] focused on local structure and conformation at the PE melt/graphite and PE melt/vacuum interfaces and presented detailed results for the mass density, conformation tensor, torsion angle distribution, and bond-order parameters in the film as a function of distance from the graphite phase. The conformations of adsorbed polymer chains and their distribution in trains, tails, and loops were also analyzed and compared to available data.[9]

* To whom correspondence should be addressed at the University of Patras, e-mail: vlasis@chemeng.upatras.gr, tel.: (+30)-2610-997 398, fax: (+30)-2610-965 223.

10.1021/ma050177j CCC: $30.25
Published on Web 06/01/2005

The work reported here addresses the issue of molecular mobility at the two interfaces. We are interested in both the short-time (local) dynamics of the melt (torsional time autocorrelation functions and local mobility) and the long-time (diffusive) motion of adsorbed segments or entire chains in the polymer matrix.

In the literature, dynamics and chain mobility in thin adsorbed films have been probed by a variety of techniques, such as dynamic secondary ion mass spectrometry (DSIMS),[16−19] fluorescence recovery after patterned photobleaching (FRAPP),[20] fluorescence nonradiative energy transfer (NRET),[21] neutron reflectometry (NR),[22] quasielastic neutron scattering (QNS),[23] and nuclear magnetic resonance (NMR).[24,25] All these methods indicate a different chain mobility of the polymer near an attractive surface than in its bulk. However, there exist significant differences in the findings of the works as far as the length scale of the phenomenon and the extent of the surface effect on the lateral motion of the chains are concerned. Zheng et al.,[16,17] for example, have studied diffusion in thin films of polystyrene (PS) using DSIMS: measured diffusion coefficients were different from those in bulk PS up to distances equal to $10R_g$ for diffusion in films adsorbed on attractive surfaces and up to distances equal to $4R_g$ for diffusion at the free surface of PS. The FRAPP measurements of Frank et al.[20] suggest that the chain self-diffusion coefficient in a PS film remains lower than in bulk PS up to distances approximately equal to the length of the fully extended chain. These findings are in contrast to the neutron reflectometry measurements of Lin et al.,[22] according to which the diffusion of poly(methyl methacrylate) (PMMA) near a strongly attractive surface recovers its bulk value within a distance approximately equal to $3R_g$ or $4R_g$. The deuterium NMR studies of Lin and Blum[24] showed that PMMA films adsorbed on silica exhibit slower segmental dynamics and greater heterogeneity in segmental mobility as opposed to segmental dynamics in the bulk of the polymer. Segmental dynamics in adsorbed PDMS chains have also been measured by Rivilon et al.,[25] who reported induced chain orientation and anisotropic chain segment dynamics even on a nonadsorbing surface.

Zheng et al.[16,17] have also reported that the chain self-diffusion coefficient in an adsorbed film scales differently with polymer molecular weight (MW) than what is predicted by the reptation theory.[26] A modified reptation theory was thus proposed for entangled polymer melts near attractive surfaces, which incorporates a value for the monomer friction coefficient slightly higher than in the bulk polymer due to chain contacts with the surface. For diffusion at the free surface of the melt, the DSIMS studies of Pu et al.[18] with PS film samples showed that the diffusion coefficient is reduced relative to the bulk value up to a distance d equal to $4R_g$ from the vacuum interface; it also scales with chain length N as $N^{-2.5}$.

Besides experiments, molecular simulations have also been used to probe polymer structure and dynamics in polymer/solid interfacial systems using dynamic Monte Carlo (MC) and MD methods.[12−15,27−42] Mansfield and Theodorou[12] carried out dynamic MC simulations on a dense liquid consisting of freely jointed 20-bead long chain molecules in a cubic lattice in the vicinity of solid walls and evaluated the self-diffusion coefficient of chains and its spatial dependence. Calculations of the mean-square center-of-mass displacement as a function of simulation time showed a dramatic reduction in chain mobility near strongly adsorbing walls over several layers, but an enhancement near weakly adsorbing walls, mainly as a result of a decrease in polymer segment density. Strong segment−wall attractive interactions were seen to appreciably prolong relaxation times, in comparison to the bulk. Bitsanis and Hadzioannou[27] performed a series of MD simulations with FENE chains to investigate structure and microscopic dynamics in thin films of homopolymer melts confined between structureless, planar solid walls. Yoon et al.[32] reported on apparent diffusion coefficients in melts of short-chain polymethylene systems near adsorbing surfaces through MD simulations with both bead−spring and atomistic models,[29−32] based on calculations of the mean-square displacement (msd) of the chain center-of-mass within short time intervals. Significant perturbations from the corresponding bulk diffusion coefficients were recorded only for chains diffusing very close to the surface (up to about 1 nm). Aoyagi et al.[33] carried out MD simulations of polymer melts confined between walls with a bead−spring model and reported on the effect of the interface on chain relaxation by analyzing the time autocorrelation functions of the normal modes as a function of distance from the wall.

Chain dynamics has also been studied in systems of polymers confined between nonadsorbing solid surfaces.[36−38] MC calculations with the bond fluctuation model showed that segmental mobility is enhanced as the film thickness is decreased, but the overall chain dynamics remains unaltered.

More recently, Borodin et al.[41] have reported new results from detailed MD simulation studies of the interface between poly(ethylene oxide) (PEO) and a TiO_2 surface using a quantum-based force field. In the simulations, layers of highly dense polymer (compared to the bulk melt) were formed that persisted up to 15 Å from the surface, accompanied by a dramatic slowdown in the conformational and structural relaxation, in comparison to bulk PEO. Borodin et al.[41] have concluded that the nature of PEO relaxation at the TiO_2 interface is determined not only by the increased polymer density at the TiO_2 surface but also by the surface topography and electrostatic interaction between PEO and TiO_2. Efforts to combine quantum methods with dynamic simulations within a hierarchical, multiscale modeling scheme in order to calculate chain and segmental dynamics at polymer/metal interfaces are also in progress today.[42]

The literature survey proves that, despite earlier and recent advances in our understanding of structural and thermodynamic properties of polymer melts at interfaces, certain issues remain unresolved. The issue of melt dynamics (especially the long-time dynamics), in particular, near an attractive surface is still unresolved: what is the spatial dependence of the diffusion or transport coefficient, D, and how D scales with chain length below and above the characteristic molecular length for the formation of entanglements, M_e, remain unanswered. This is related to the problem of long relaxation times plaguing the majority of brute-force dynamics methods employed to probe chain dynamics at interfaces; as a consequence, atomistic-level MD simulations of interfacial dynamics have so far been restricted to relatively short-chain systems (MW less than or up to M_e) and for times that hardly exceed 16 ns. In the present work, new results are presented for

the dynamic and transport properties of polymer melts at interfaces, through a hierarchical approach that allowed us to simulate significantly larger chain systems and access longer simulation times. The data have been accumulated from detailed MD simulations with three different PE systems, of molecular length C_{78}, C_{156}, and C_{250}, adsorbed on a graphite phase on the one side and exposed to vacuum on the other.[9] Keys to the success of our work are (a) the use in the simulations of a detailed atomistic force field which offers an accurate description of the polymer melt density and chain conformation, (b) the generation of realistic atomistic configurations fully representative of the adsorbed melt, and (c) the consistent calculation of the transport properties of the adsorbed film through mapping of the MD trajectories for the diffusion of a population of "tagged" segments or "walkers" in the film onto the solution of a macroscopic continuum diffusion equation.

The paper is organized as follows: Section II reviews the molecular model and the methodology followed to generate well-relaxed configurations of adsorbed PE melt films and simulate their dynamic properties. Section III presents results concerning the local dynamics of the simulated systems, especially their torsional dynamics; it also includes a detailed discussion of their incoherent dynamic structure factor. The computational strategy followed to extract the long-time, transport properties of the interfacial system and results concerning the diffusive motion of adsorbed segments are presented in section IV. Section V summarizes our findings and major conclusions and discusses plans for future work.

II. The Model

The physical system we studied in this and the preceding paper[9] is that of a dense, multichain PE melt adsorbed on graphite on the one side and exposed to vacuum on the other. Polymer chains are modeled as consisting of atoms in the united-atom representation, according to which each methylene and methyl group along the main chain backbone is considered as a single LJ interacting site. The simulation box or unit cell, at the two sides of which the graphite and vacuum interfaces are located, is orthorhombic. Along the x and y directions of the coordinate system, periodic boundary conditions are implemented; i.e., the system behaves as infinite there. Through this, a thin film of liquid of effectively infinite extent along x and y and finite width along the third (z) direction is formed. The film is built sufficiently thick so as (a) to contain a region far from the two interfaces whose structural, dynamic and thermodynamic properties are identical to that of bulk polymer in all aspects and (b) to ensure that the effects of the two interfaces are isolated. These two requirements are met if the size of the film in the z direction, L_z, is about 4−5 times larger than the root-mean-square radius-of-gyration of the chains in the bulk, R_g. On the other hand, to reliably calculate transport properties, one needs to monitor the msd of atoms for times significantly longer than the longest relaxation time in the bulk, τ_1. For unentangled melts, τ_1 is of the same order as the Rouse time, τ_R, whereas for entangled melts, τ_1 is on the order of the chain disentanglement time, τ_d. Thus, most of the conclusions referring to the diffusive properties of the confined PE melts have been obtained here from a simulation with a truly "large" 200-chain C_{78} PE melt, of thickness L_z approximately equal to $17R_g$.

Table 1. Details of the Adsorbed PE Melts Simulated in This Work

chain length, N	number of chains, N_{ch}	notation	simulation time, t (ns)
78	50	C_{78} PE film	40
78	200	"large" C_{78} PE film	40
156	48	C_{156} PE film	70
250	48	C_{250} PE film	100

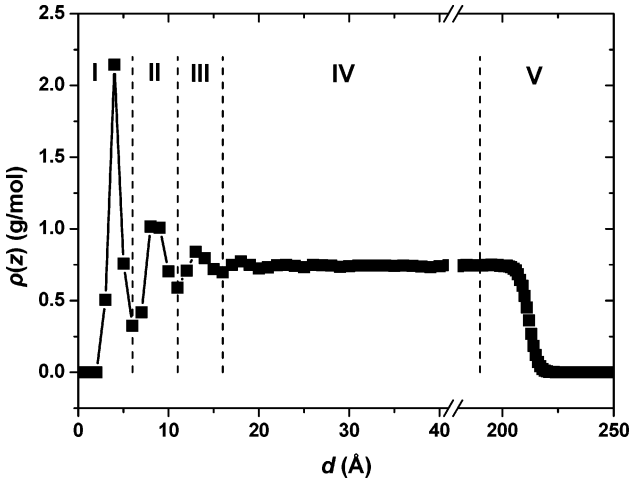

Figure 1. Density profile along the z direction of the "large" C_{78} PE film. The spatial dependence of the short-time dynamical characteristics of the film is resolved by analyzing the simulation results separately in each one of the five representative zones (I, II, III, IV, and V) defined in the figure by the vertical dashed lines.

In the simulations, adjacent methyl and methylene groups along each chain backbone are maintained at a fixed distance l, bond angles are assumed to fluctuate around an equilibrium angle subject to the van der Ploeg and Berendsen potential,[43] dihedral angles are subjected to the torsional potential of Toxvaerd,[44] and nonbonded interactions are described by a 6−12 LJ potential.[45,46] To model the polymer melt/graphite interface, Steele's potential has been used.[11]

All results reported in this work have been based on MD simulations conducted in the NPT equilibrium ensemble, at $T = 450$ K and $P = 0$ atm. Most data have been accumulated from simulations with two different, strictly monodisperse, unentangled PE systems: The first consists of 50 chains of length C_{78} and the second of 48 chains of length C_{156}. To quantify the effect of the confining boundary on conformational relaxation, we also carried out an MD simulation with a longer system consisting of 48 chains of length C_{250}. On the other hand, to study transport properties along the z direction of the film and keep the effects of the two interfaces isolated, a long MD simulation was also executed with a very large C_{78} system containing 200 chains in the simulation box; we will refer to this in the following as the "large" C_{78} system. The total duration of the MD runs was 40 ns for the C_{78} system, 70 ns for the C_{156} system, 100 ns for the C_{250} system, and 40 ns for the large C_{78} system. A detailed description (chain length, number of chains, simulation time) of all simulated systems is given in Table 1.

As an example of the local mass density normal to the graphite surface, discussed in detail in the first part of this work,[9] Figure 1 presents the density profile $\rho = \rho(z)$ characterizing the large 200-chain C_{78} melt; strong PE structuring is indicated in the figure up to ap-

proximately 18 Å from the substrate. Beyond 18 Å, the profile assumes an asymptotic form characteristic of a system with a constant local mass density, equal to that of bulk PE, up to positions where the free surface of the melt is encountered (at the melt/vacuum interface). The melt free surface is depleted in polymer mass, and the density profile attains the characteristic sigmoidal shape, dropping gradually from the bulk value to zero at the extreme edge of the film.

Motivated by the oscillatory structure of the density profile, the interfacial area can be divided into five (5) distinct "zones" or "regions", using as guides the minima of the local mass density distribution. The five zones are shown in Figure 1 by the vertical dashed lines and will be very helpful in our analysis of the dynamic properties of the melt at the two interfaces.

In addition to local mass density and other descriptors of the local structure and chain conformation in PE melts confined between the graphite and vacuum interfaces discussed in detail in our previous contributiton,[9] information on how chain mobility and relaxation is affected by the presence of the adsorbing solid surface is also of paramount importance. These determine the viscoelastic properties of the confined film, which, in turn, govern its response to an applied flow field, such as shear. Results about these properties and a comparison against those of the corresponding bulk polymer melt are presented and discussed in detail in the next paragraphs of the present paper. In all cases, analyzing the simulation results spatially has been accomplished by assigning each piece of the dynamical information under study to one of the five regions of the film defined above, based on the position of the z coordinate of the element (torsion angle or segment) at the time origin.

III. Local Dynamics

A. Torsional Relaxation. Local dynamics in the interfacial system can be quantified in terms of the torsional time autocorrelation function (TACF), defined as

$$P(\phi(t)) = \frac{\langle \cos \phi(t) \cos \phi(0) \rangle - \langle \cos \phi(0) \rangle^2}{\langle \cos \phi(0) \cos \phi(0) \rangle - \langle \cos \phi(0) \rangle^2} \qquad (1)$$

with the brackets denoting an ensemble average over all available torsion angles $\phi(t)$. The decay of $P(\phi(t))$ for torsion angles belonging to each of the five regions defined in Figure 1 is shown in Figure 2a for the C_{78} PE melt film and in Figure 2b for the C_{156} one. Also shown in the figures with the open circles are the corresponding bulk profiles. The following observations can be made: (a) in region I (which coincides with the first adsorption layer in the density profile), local dynamics is considerably slower than in the bulk; (b) in regions II, III, and IV of the film, torsional dynamics is indistinguishable from that observed in the unconstrained bulk polymer; and (c) at the free surface of the melt (region V), local dynamics is considerable faster than in the bulk. The latter effect is a result of the decrease in polymer segment density. The curves of Figure 2a,b can be accurately fitted with stretched exponential functions of the form $P(\phi(t)) = \exp(-(t/t_{KWW})^{\beta})$, where t_{KWW} is a characteristic relaxation time and β a factor accounting for deviation from the Debye behavior. Values for the characteristic relaxation times t_{KWW} and stretching exponents β that provide the best fits to the simulation data and their spatial resolution

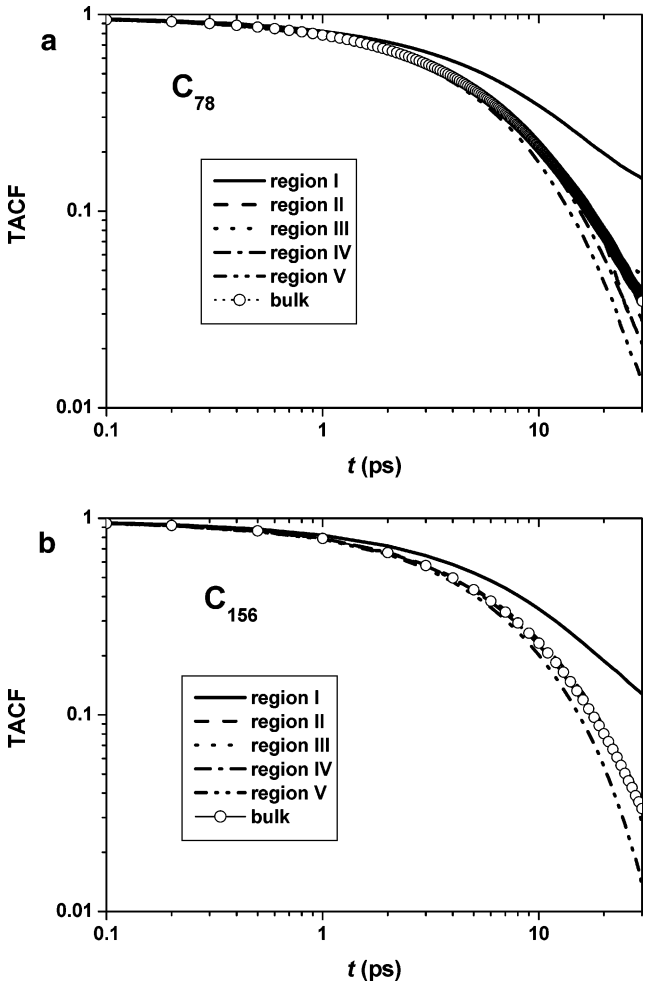

Figure 2. Torsional time autocorrelation function for two chain length systems, C_{78} (a) and C_{156} (b), and their spatial dependence. Shown by the circles are the curves obtained from MD simulations with the corresponding bulk melts.

are summarized in Table 2. It is concluded that the influence of the graphite phase on the conformational relaxation of adsorbed PE is very local: it is limited to the first adsorption layer extending up to only 5 Å from the surface, whereas for torsion angles beyond 5 Å, it is identical to that in bulk polymer. A similar conclusion has been reported by Borodin et al.[41] for the local relaxation of PEO at the TiO_2 surface.

How conformational dynamics in the first adsorption layer and in the bulk polymer depends on the MW of the melt is shown in Figure 3. Local dynamics in the smaller-MW system, C_{78}, is somewhat faster than in the two higher-MW systems, C_{156} and C_{250}. For even longer systems, differences in torsional time autocorrelation functions diminish, and eventually, the conformational relaxation becomes MW-independent.

B. Local Mobility in the *xy* Plane, Parallel to Graphite and Vacuum Interfaces. As a measure of local mobility in our confined systems, we used the msd of segments along the x and y directions as a function of distance from the graphite phase. For convenience, segmental displacements were calculated only for the five characteristic regions defined in the previous sections (based on the loci of the local density minima in Figure 1). Segmental displacements in our work were calculated as follows: First, the z component of each segment at the beginning of the time sweep was recorded and assigned to the appropriate region. Next,

Table 2. Values of the Characteristic Kohlrausch–Williams–Watts Relaxation Times t_{KWW} (in ps) and Stretching Exponents β, Obtained from Fits of the Torsional Time Autocorrelation Functions and Their Spatial Dependence, as a Function of Chain Length[a]

		C_{78}		C_{156}		C_{250}	
region	range, Å	t_{KWW}	β	t_{KWW}	β	t_{KWW}	β
I	0–6	9.8 ± 0.2	0.68	10.1 ± 0.2	0.78	10.8 ± 0.2	0.78
II	6–12	5.8 ± 0.1	0.75	5.9 ± 0.1	0.81	6.0 ± 0.1	0.82
III	12–19	5.5 ± 0.1	0.80	5.6 ± 0.1	0.82	5.9 ± 0.1	0.82
IV	19–(L_z–25)	5.5 ± 0.1	0.82	5.6 ± 0.1	0.81	5.7 ± 0.1	0.81
V	(L_z–25)–L_z	5.2 ± 0.1	0.85	5.3 ± 0.1	0.84	5.4 ± 0.1	0.84
bulk		5.45 ± 0.1	0.82	5.6 ± 0.1	0.82	5.65 ± 0.1	0.82

[a] Also reported for comparison are the values of the two parameters in the corresponding bulk melts [L_z is the length of the simulated film in the z direction].

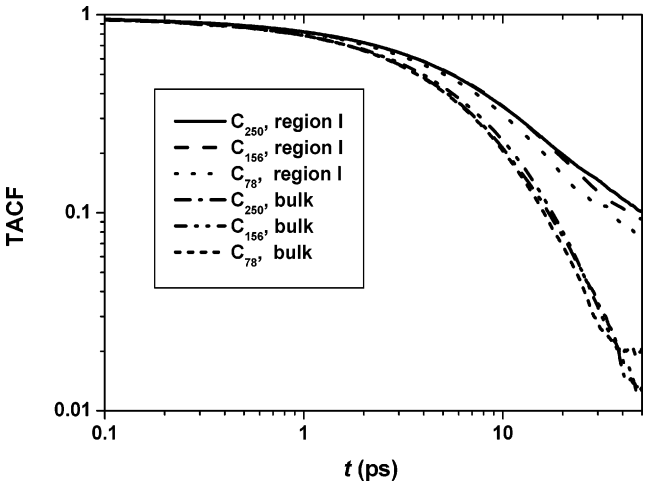

Figure 3. Torsional time autocorrelation function in regions I and IV of the simulated films, corresponding to the first adsorption layer and their bulklike zone, respectively, as a function of chain length.

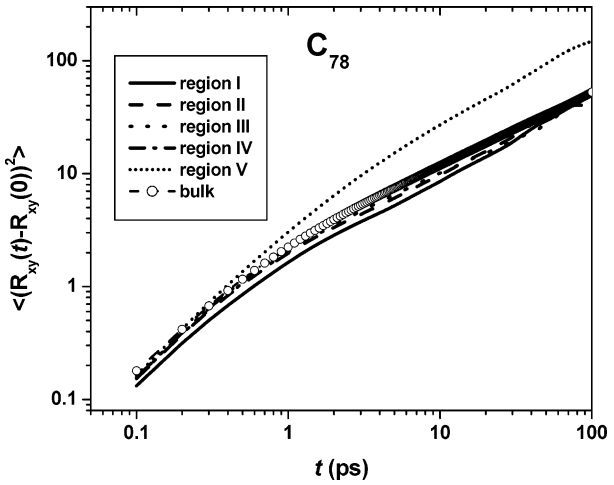

Figure 4. Mean-square displacement (msd) of carbon atoms in the xy plane as a function of time, at various positions in the film, for the adsorbed C_{78} PE melt. Symbols account for the msd curve in the bulk, unconstrained C_{78} melt.

during the MD simulation, the new positions of all segments were recorded as a function of time and assigned again to one of the five regions. A segment i contributes to the averaged msd $g^{(j)}(\tau)$ accumulated for a given time interval τ in region j if and only if it was constantly present in that region in the entire course of time τ. Consequently, the function $g^{(j)}(\tau)$ is calculated through

$$g^{(j)}(\tau) = \frac{1}{N_j}\sum_{i=1}^{N_j}[(R_x(i,t) - R_x(i,t_1))^2 + (R_y(i,t) - R_y(i,t_1))^2] \quad (2)$$

where $t \in (t_1, t_2)$, $\tau = t - t_1$, and N_j is the number of atoms continuously belonging to region j in the course of time τ. Since the probability for an atom to leave the bin or region it was assigned to at the time origin increases rapidly with time, the functions $g^{(j)}(\tau)$ are presented here for rather short time separations, on the order of a few hundreds of picoseconds.

Logarithmic plots of the functions $g^{(j)}(\tau)$ for the C_{78} film and their spatial dependence are shown in Figure 4. For comparison, also shown in the figure are the segmental displacements as obtained from an MD simulation with a bulk, unconstrained C_{78} PE melt system, at the same temperature. The figure demonstrates that PE carbon atoms adsorbed in region I (closest to the graphite phase) exhibit a slower dynamics than carbon atoms in all other regions. In fact, segmental mobilities in regions II, III, and IV of the film are very similar with each other and practically indistinguishable from that in the bulk melt. On the other hand, the overall displacement of segments in region V (the melt free surface) is significantly enhanced compared to the bulk. This is a purely density effect; it persists up to 20 Å from the outer edge of the film and is quickly suppressed as one moves toward the bulk. Quite similar plots have been obtained with the rest of the simulated systems.

As mentioned in section 1, experimentally, structural relaxation in a polymer melt at attractive surfaces is investigated with techniques such as quasi-elastic neutron scattering (QNS) and neutron spin echo (NSE). Data from NSE experiments for the dynamic structure factor, in particular, are directly comparable to our MD simulation data for the single chain coherent or incoherent dynamic structure factor. Structural relaxation here is separately examined in each one of the five representative regions defined in Figure 1, ranging from I (the first adsorption layer) to V (the free surface), through calculations of the incoherent (self-) dynamic structure factor along the xy plane:[26]

$$S^{xy}_{inc}(q,t) = \langle \exp[i\mathbf{q}\cdot\Delta\mathbf{R}^{xy}(t)]\rangle \quad (3)$$

In eq 3, $\mathbf{q}$ is the momentum transfer vector, q its magnitude, and $\Delta\mathbf{R}^{xy}(t)$ the atom displacement vector in the xy plane after time t, $\Delta\mathbf{R}^{xy}(t) = \mathbf{R}^{xy}(t) - \mathbf{R}^{xy}(0)$, while brackets denote an average over all atoms constantly present in the characteristic region in the course of time t. For isotropic motion, eq 3 reduces to

$$S^{xy}_{\mathrm{inc}}(q,t) = \langle \cos(\Delta \mathbf{R}^{xy})\cdot\mathbf{q}\rangle = \frac{1}{2\pi}\left\langle \int_0^{2\pi} \cos[q\Delta R^{xy}(t)\cos\theta]\, \mathrm{d}\theta \right\rangle \quad (4)$$

where ΔR^{xy} is the magnitude of $\Delta \mathbf{R}^{xy}$. By further assuming that the magnitude of the segmental displacements follows a Gaussian distribution, the incoherent dynamics structure factor simplifies to[26]

$$S^{xy}_{\mathrm{inc-Gauss}}(q,t) = \exp\left(-\frac{q^2}{4}\langle \Delta R^{xy}(t)^2\rangle\right) \quad (5)$$

The leading-term correction to the non-Gaussian behavior is given by[47]

$$S^{xy}_{\mathrm{inc}}(q,t) = S^{xy}_{\mathrm{inc-Gauss}}(q,t)\left[1 + \frac{1}{2}\left(\frac{q^2}{4}\langle \Delta R^{xy}(t)^2\rangle\right)\alpha_2(t)\right] \quad (6)$$

where

$$\alpha_2(t) = \frac{3\langle \Delta R^{xy}(t)^4\rangle}{5\langle \Delta R^{xy}(t)^2\rangle^2} - 1 \quad (7)$$

Equation 4 permits calculating $S^{xy}_{\mathrm{inc}}(t)$ and its spatial dependence directly from our MD simulations. To improve statistics, we have made use of the technique of multiple time origins, with time origins in our computations chosen every 1 ps. We have also averaged over a large number of possible directions of the **q** vector. All results presented here have been obtained for a value of the magnitude of the **q** vector equal to 1.35 Å^{-1} (as defined by the position of the first peak in the pattern of the static structure factor) and by averaging over 120 possible wavevector directions, equally spaced in the *xy* plane.[40] Figure 5a,b shows how S^{xy}_{inc} changes in each one of the five characteristic regions of the film in the *z* direction, from our MD simulations with the C_{78} and the C_{250} PE melt films. Consistently with the data for the segmental displacements in the *xy* plane, structural relaxation is slowest in region I (right next to the graphite phase). In contrast, in regions II and III, and in the bulk zone of the film (region IV), it is practically invariant and almost indistinguishable from those in a bulk PE melt of the same MW. The polymer/vacuum interface (region V) is characterized by a faster segmental mobility, as a consequence of the lower density prevailing there.

Figure 6 tests the validity of the Gaussian approximation by presenting S^{xy}_{inc} plots obtained by making use of eq 5 (incorporating the Gaussian approximation) and of eq 6 (incorporating the Gaussian approximation but corrected up to the first order). For convenience, only the curves for regions I and IV of the film are shown. For very short times or small *q* values such that $q^2\langle \Delta R^{xy}(t)^2\rangle$ is smaller than 1, both methods give similar S^{xy}_{inc} predictions. For longer times, however, the Gaussian approximation breaks down, and corrections are definitely needed in the calculation of S^{xy}_{inc} to capture heterogeneities in segmental dynamics. Qualitatively similar results have been reported by Borodin et al.[41] based on MD simulations with a bead model.

In addition to structural relaxation, chain molecular mobility in the adsorbed films in the plane parallel to the graphite phase is also of great importance, since it provides information about the transport properties of the confined melt. This is examined here through the

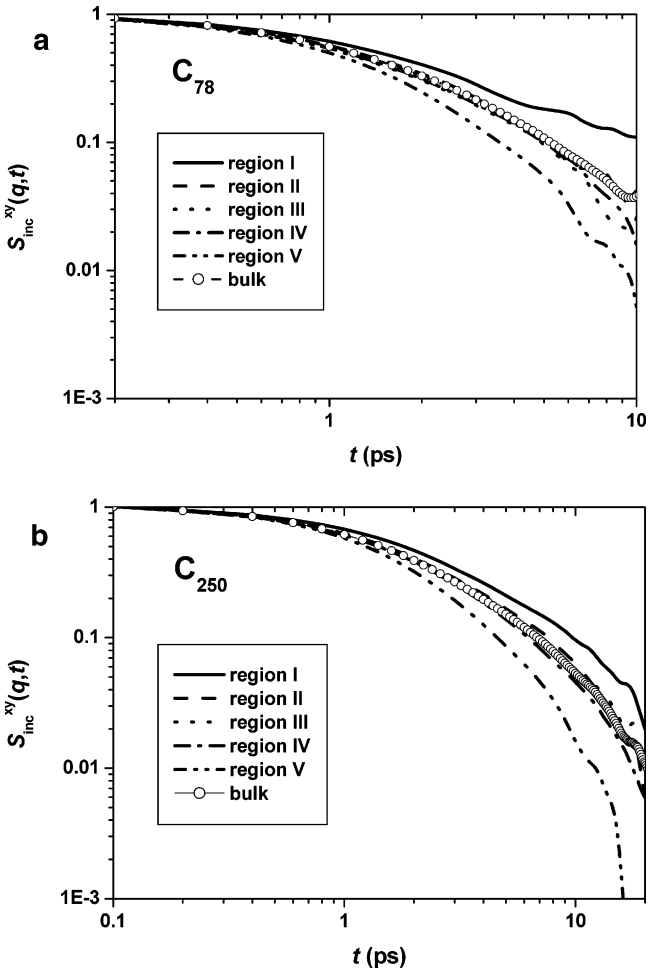

Figure 5. Spatial dependence of the incoherent dynamic intermediate structure factor, $S^{xy}_{\mathrm{inc}}(t)$, for the adsorbed C_{78} (a) and C_{250} (b) PE systems. All patterns have been calculated for a value of the magnitude *q* of the wavevector **q** equal to 1.35 Å^{-1}.

definition of a tensorial apparent diffusion coefficient, $\mathbf{D}_{\mathrm{app}}$, based on the chain center-of-mass msd and its spatial dependence along *z* within a given, short time interval. The diagonal components of $\mathbf{D}_{\mathrm{app}}$ are defined according to

$$D_{\mathrm{app},a}(z) = \frac{1}{6t_c}\langle (R_{cm,a}(z, t + t_c) - R_{cm,a}(z, t))^2\rangle \quad (8)$$

where $R_{cm,a}(z, t + t_c)$ represents the *a*th (*x*, *y*, or *z*) component of the chain center-of-mass position at time $t + t_c$, which at time *t* was a distance *z* form the solid surface, and t_c is a predefined time constant. For the systems simulated here, apparent chain center-of-mass diffusivities, $\mathbf{D}_{\mathrm{app}}(z)$, calculated for various values of the characteristic short diffusion time t_c, were seen to be invariant only for observation times up to 2 ps; thus, t_c = 2 ps in all results presented below.

The tensor of chain center-of-mass apparent diffusivity, $\mathbf{D}_{\mathrm{app}}(z)$, was calculated as a function of position with respect to the graphite phase by partitioning space along *z* into parallel layers, or bins, of width 1 Å each. Results for the C_{78} and C_{156} PE films are shown in parts a and b of Figure 7, respectively. Because of symmetry, $D_{\mathrm{app},x} = D_{\mathrm{app},y}$ for all bins; thus, only the *x* and *z* components of the total chain self-diffusivity tensor $\mathbf{D}_{\mathrm{app}}$ are shown

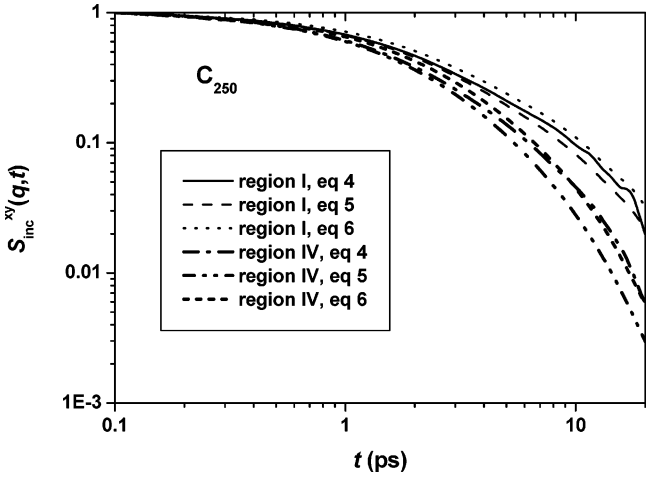

Figure 6. Patterns of the incoherent intermediate structure factor, $S_{inc}^{xy}(t)$, in regions I and IV of the C_{250} film, corresponding to the first adsorption layer and its bulklike zone, respectively. Solid lines correspond to $S_{inc}^{xy}(t)$ patterns obtained directly from the MD simulations using eq 4, whereas dashed and dotted lines are the predictions of eqs 5 and 6, based on the use of the Gaussian approximation without and with the first-order term correction, respectively. All patterns have been calculated for a value of the magnitude q of the wavevector $\mathbf{q}$ equal to 1.35 Å^{-1}.

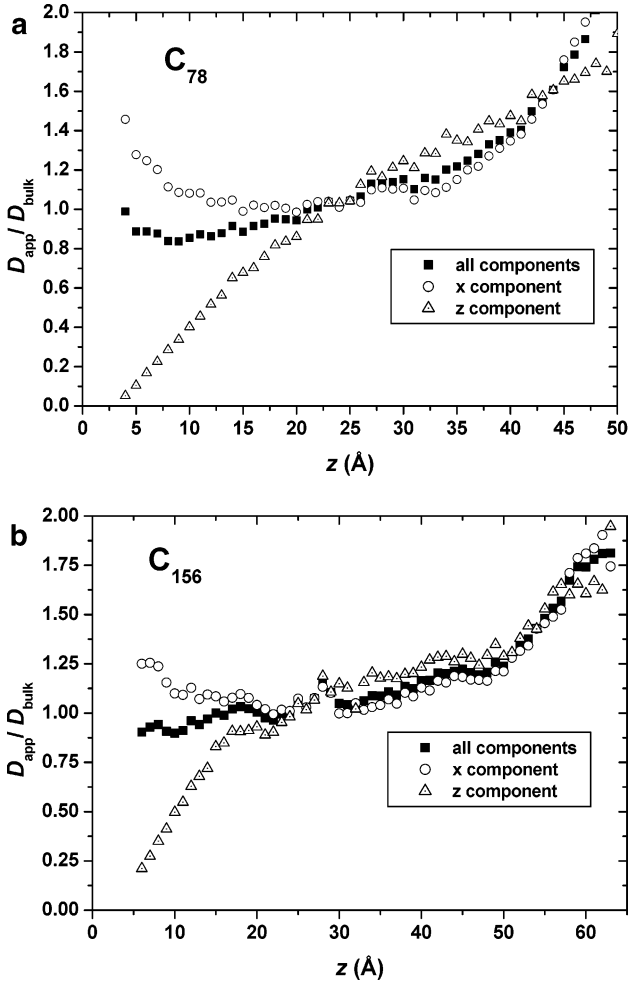

Figure 7. Spatial dependence of the apparent diffusion coefficient $\mathbf{D}_{app}$ (filled squares) and its x (open circles) and z (open triangles) components, for the adsorbed C_{78} (a) and C_{156} (b) PE melt films. Results in each bin have been averaged over those chains that did not leave the bin to which they were assigned at the time origin during the time sweep. All diffusivity values have been scaled with their values in the bulk, unconstrained melt of the same chain length.

in the figures, scaled with the value of D_{app} obtained from additional MD simulations with bulk (i.e., unconstrained) systems of the same MW.[48−51] In agreement with the results of previous dynamic studies with simpler models on shorter chain melt systems,[32] the diffusive motion of chains is highly anisotropic in the interfacial area: up to about 25 Å from the graphite phase, $D_{app,z}$ is significantly smaller than $D_{app,x}$ and $D_{app,y}$. It is also remarkable that in this regime ($z \leq 25$ Å) $D_{app,x}$ and $D_{app,y}$ are larger than 1; i.e., molecular diffusion and migration is accelerated along the x and y directions but is slowed down along the z direction, relative to the bulk. This result, which has also been observed in past simulations of short-chain melts near nonadsorbing walls or weakly adsorbing surfaces,[12,32] is attributed to the lower *mean* density characterizing the film for distances less than 25 Å from the graphite surface relative to the bulk system: indeed, despite the maxima of the local mass density in the interfacial area, its mean value over the first 25 Å is 0.694 g/cm^3 for the C_{78} and 0.705 g/cm^3 for the C_{156} PE melt systems, i.e., smaller than the corresponding bulk densities in the two systems (0.74 and 0.75 g/cm^3, respectively). At distances beyond 25 Å from the graphite phase, $\mathbf{D}_{app}$ becomes isotropic ($D_{app,x} = D_{app,y} = D_{app,z}$); in addition, its value rises continuously with increasing distance from the surface so that, beyond 30 Å, $\mathbf{D}_{app}$ exceeds its value in the unconstrained bulk phase of the melt of the same MW. In fact, at the outer (polymer/vacuum) interface, chain mobility is considerably enhanced, and $\mathbf{D}_{app}$ (which continues to remain isotropic) rises steeply to assume values up to 2 times larger than in the bulk.

Figure 7a,b shows that the overall effect of the graphite phase is a decrease in the z component of the total chain diffusivity over several layers close to the surface. As a result, the width of the simulated 50-chain C_{78} and 48-chain C_{156} PE melts systems appears too small for the two systems to exhibit a distinct bulklike zone as far as aspects of chain mobility are concerned. This should be contrasted to structural and thermodynamic aspects in these model films, which vary over shorter length scales, so that in the middle region (region IV) they become practically indistinguishable from those of the corresponding unconstrained melts.[9] We consider these models as ultrathin films of the corresponding adsorbed melts. To build models of adsorbed PE melts with a clearly defined middle zone of bulklike features in all aspects (structural, conformational, thermodynamic, and dynamic), the size of the z dimension of the simulation box, L_z, should be considerably larger. We built such a "large" system here by generating[15] chains of C_{78} PE in an orthorhombic unit cell (simulation box) of dimensions $L_x = 49.4$ Å, $L_y = 46.87$ Å, and $L_z = 240$ Å (with its two edges exposed again to graphite and vacuum, respectively). The resulting model was subjected to a long MD simulation for more than 40 ns, and the results obtained for the spatial dependence of the three components of $\mathbf{D}_{app}$ are shown in Figure 8. Again, since $D_{app,x} = D_{app,y}$, only its x and z components are shown, scaled with the bulk $\mathbf{D}_{app}$ value for the C_{78} PE at $T = 450$ K. For distances up to 25 Å from the graphite surface, $D_{app,x}$ and $D_{app,z}$ in the thin and large C_{78} melts vary identically with position z from the surface. In contrast, however, to the thin film, the

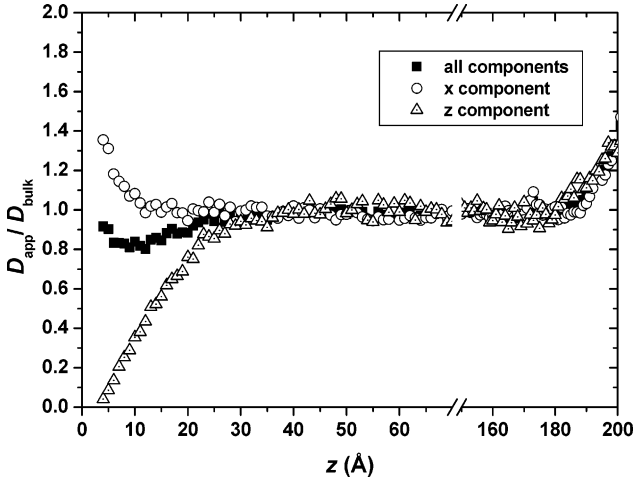

Figure 8. Same as with Figure 7a but for the "large" C_{78} PE melt.

large C_{78} model possesses a well-defined, broad middle zone, across which all three components of $\mathbf{D}_{app}$ assume the same value, equal to that monitored in an unconstrained C_{78} PE melt. The middle zone of this larger C_{78} PE film can therefore be considered as truly representative of a bulklike C_{78} PE melt in all system aspects.

The data reported above for the spatial dependence of the three components of the apparent diffusivity tensor are significant in their own, since they reveal the inhomogeneous and highly anisotropic character of chain mobility at the graphite surface on time scales on the order of a few picoseconds. In real applications, however, one is interested in the diffusive motion of tracer or adsorbed polymer atoms normal to the surface on time scales on the order of or longer than the chain longest relaxation time. This happens because the longest relaxation time (the characteristic time over which a section of the chain equal to its end-to-end distance retains memory of its original conformation) is intimately related to the viscoelastic behavior exhibited by the polymer fluid under the application of a flow field. For unentangled melts, this time is equal to the Rouse time; for entangled melts, it is equal to the chain disentanglement time from the tube constraints. Zheng et al.,[16] for example, used SIMS to measure tracer diffusion coefficients near polystyrene (PS) melt−solid interfaces and quantify their dependence on the degree of polymerization of the adsorbed PS chain molecules. On the basis of these measurements, a modified reptation theory was proposed that accounts for the increased friction due to surface−monomer contacts. Knowledge of monomer or tracer diffusivity is also important in applications involving polymerization reactions at the active sites of a nanopore, typically encountered in the course of polyolefin synthesis with heterogeneous supported catalysts.[52−54] How one can analyze MD runs to calculate the long-time diffusive properties of adsorbed PE melts such as those simulated here is presented and discussed in the next section of this paper.

IV. Long-Time Segmental Displacement and Diffusion in the *z* Direction, Perpendicular to Graphite and Vacuum Interfaces

Analyzing MD trajectories of multichain melt systems in confined geometries such as the adsorbed PE films studied here in order to extract their long-time diffusive properties presents a number of difficulties. These are related to (a) the inherent limitations of the MD technique in vigorously sampling the configuration space of highly connected dense systems,[48−51] (b) the fact that segments and chains diffuse in restricted volume and therefore cannot achieve the Einstein limit for diffusion due to the presence of boundaries,[55] and (c) the anisotropic and inhomogeneous character of the motion at the interface.[55] Even if we are interested only in the diffusion coefficient perpendicular to the confining boundary, the diffusive motion depends strongly on mass location across the film, which cannot be neglected in the analysis.

To address transport phenomena in adsorbed melts such as the thin and ultrathin PE films studied here, a new approach is proposed and implemented based on a method that monitors a population of "tagged" carbon atoms or walkers and records their positions along the z direction as they diffuse across the film due to thermal agitation. Such an approach allows one to follow the concentration of "tagged" atoms in space as a function of time and then to extract the value of the underlying effective diffusion constant, D, by mapping the resulting profiles onto the solution of a macroscopic diffusion equation. The method is an excellent alternative to the more sophisticated one based on the slope of the msd of the diffusant particles in the limit (Einstein or Fickian) of infinitely long times. For bulk polymers, of course, both methods give identical results, as will also be demonstrated below. Unfortunately, for confined systems, the Einstein limit is never reached; in this case, the new approach provides an excellent alternative method to get at the transport properties of the adsorbed melt.[55]

According to the proposed strategy, the diffusion of adsorbed carbon atoms in the polymer film obeys an unsteady 1-d diffusion equation of the following form:[26]

$$\frac{\partial C}{\partial t} = \frac{\partial}{\partial z}\frac{D}{k_B T}\left(k_B T \frac{\partial C}{\partial z} + C\frac{\partial U}{\partial z}\right) \tag{9}$$

In eq 9, C denotes the concentration of tagged molecules at time t and position z in the external field or potential $U(z)$ caused by the rest of segments and the confining boundary, and D their effective diffusion or transport coefficient. Equation 9 provides a macroscopic description to the dynamics of the diffusing Brownian particles and dates back to the pioneering works of Einstein on Brownian motion. It is based on the assumption that if the concentration is not uniform, there is a flux which is proportional to the spatial gradient of the concentration (Fick's law of diffusion).[56]

Given the short-range of the potential describing polymer−surface interactions, neglecting mean-field effects and assuming that D does not depend on local position z, eq 9 can simplify to

$$\frac{\partial C(t,z)}{\partial t} = D\frac{\partial^2 C(t,z)}{\partial z^2} \tag{10}$$

subject to the following initial and boundary conditions: (i) at $t = 0$ (initial condition): $C(t,z) = f(z)$, where $f(z)$ describes the initial concentration of tagged molecules (walkers) in the film; (ii) at $z = \infty$ (boundary condition): $C(t,z) = 0$ (semiinfinite medium assump-

tion); and (iii) at $z = 0$: $\partial C(t,z)/\partial z = 0$ (zero flux assumption on the wall).

The general solution to the initial-boundary value (ibv) problem defined by eq 10 is given by[57]

$$C(z,t) = \frac{1}{\sqrt{4\pi Dt}}\left(\int_0^\infty f(z') \exp\left[-\left(\frac{z-z'}{\sqrt{4Dt}}\right)^2\right] dz' + \int_0^\infty f(z') \exp\left[-\left(\frac{z+z'}{\sqrt{4Dt}}\right)^2\right] dz'\right) \quad (11)$$

Equation 11 is valid for diffusion in a semiinfinite medium and will be employed here, in conjunction with the simulation data for the "large" C_{78} system whose thickness in the z direction (almost $17R_g$) guarantees the existence of a well-defined bulklike regime in all aspects, to calculate the diffusion coefficient D of adsorbed PE segments in the vicinity of the graphite phase.

The function $f(z)$ in eq 11 defining the initial distribution of tagged atoms is imposed from the simulation data. In general, $f(z)$ will be a complicated function (due to the strong spatial dependence of the density profile at the PE/graphite interface); thus, the two integrals in eq 11 will have to be evaluated numerically.

Overall, the methodology of calculating the transport properties of the simulated adsorbed films (i.e., the diffusion constant D in the z direction normal to graphite) involves the following steps:

1. Execution of a *long* MD simulation with a model PE/graphite system whose thickness is large enough to ensure the existence of a true bulklike region in all aspects (thermodynamic, structural, conformational, and dynamic). The 200-chain C_{78}/graphite melt with $L_z = 240$ Å ($\approx 17R_g$) considered here is such a system.

2. Definition of the initial ($t = 0$) distribution of tagged atoms, $f(z)$. In the cases investigated here, the function $f(z)$ was always taken such that the selected population of "tagged" segments included all carbon atoms belonging to a region of the interfacial film extending up to a distance d from the graphite plane ($z = 0$). For the 200-chain C_{78}/graphite system, for example, typical plots of the function $f(z)$ corresponding to $d = 6$ Å (the case where one is interested in the overall mobility of atoms belonging only to the first adsorption layer), $d = 11$ Å (the case where one is interested in the overall mobility of atoms belonging to the first two adsorption layers), and $d = 17$ Å (the case where one is interested in the overall mobility of atoms belonging to all three adsorption layers) are shown in Figure 9.

3. Analysis of the MD trajectory and calculation of the corresponding concentration profiles $C_{MD}(z,t)$ of "tagged" atoms at all subsequent times ($t > 0$). To this end, concentration profiles of adsorbed carbon atoms obtained in the course of the MD simulation are documented as $C_{MD}(z_i,t)$, where $i = 1, 2, ..., N_b$, by calculating the number of carbon atoms that at time t reside in each one of the N_b bins (of thickness 5 Å each) into which the z dimension of the film is partitioned.

4. Estimation of the diffusion coefficient D through minimization of the objective function F defined according to $F(D) = \sum_{i=1}^{N_b}[C_{diff}(z_i,t;D) - C_{MD}(z_i,t)]^2$, where $C_{diff}(z,t;D)$ is the concentration profile calculated numerically[58] according to eq 11, for a given value of D.

A unique feature of the new approach is its capability to characterize segmental mobility as a function of the width or thickness d of the chosen interfacial region segments belonged to at the beginning of the diffusive process, by properly choosing $f(z)$. For example, by defining $f(z)$ to include first only the carbon atoms of the first adsorption layer (by choosing $d = 6$ Å) and then the carbon atoms of both the first and second adsorption layers (by choosing $d = 11$ Å), one can investigate whether segmental mobilities in the two layers differ and to what extent.

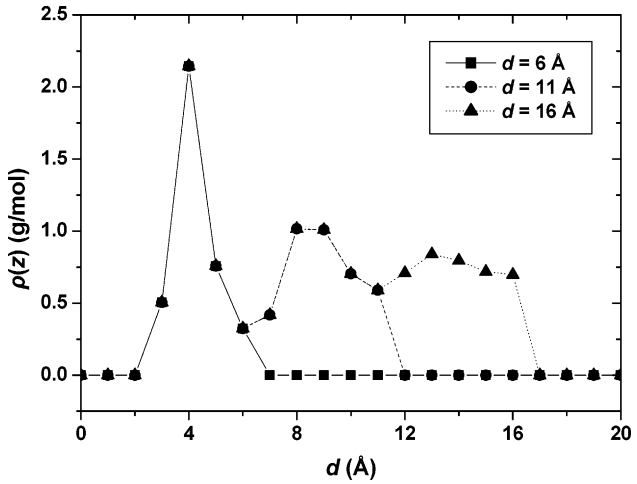

Figure 9. Initial distribution (i.e., profile of function $f(z)$) of "tagged" atoms in the large C_{78} PE melt film, for the cases $d = 6$ Å, $d = 11$ Å, and $d = 17$ Å.

If the diffusion was Fickian, the same value of D in eq 11 would fit the concentration profiles obtained from the MD simulation at all times $t > 0$. Unfortunately, segmental diffusion in the confined film is too complicated to allow the calculation of a single D value that could satisfactorily match concentration profiles at all times. To overcome this, we considered the diffusion coefficient D to be time-dependent, i.e., $D = D(t)$; then, at each time instance t, D was calculated by minimizing the objective function F only for the concentration profile at that time t. In all data presented here, D is therefore considered as a function of both the initial distribution of walkers, i.e., the width or thickness d from the graphite phase of the region under study, and time t.

To test the validity of the new method of computing diffusivities, we first employed it in calculations of the diffusion constant D of backbone carbon atoms in systems of bulk, unconstrained PE melts. Representative results from these calculations with two PE melts of length C_{156} and C_{250}, respectively, are shown in Figure 10. Figure 10a presents normalized concentration profiles obtained from calculations with a bulk population of C_{156} backbone carbon atoms that initially resided in a 10 Å thick region, at times 1, 10, 20, and 50 ns from the time origin. To improve statistics, averaging over all three directions (x, y, and z) of the coordinate system was employed, since diffusion in the bulk is homogeneous and isotropic. The best fits to the MD data based on the solution of the continuum diffusion equation (which in the bulk admits a closed-form solution due to the simple form of the function $f(z)$ specifying the initial condition[59]) are shown in the figure by the dashed curves. Similar plots are obtained from our calculations with the bulk C_{250} PE melt. The time dependence of the segmental diffusivity D in both melts is shown in Figure 10b. Even in these infinitely long (bulk) systems, diffusion is not Fickian at all times: Starting from a high value at $t = 0$, D decreases monotonically with time (anomalous diffusion regime)[56] over a time scale which

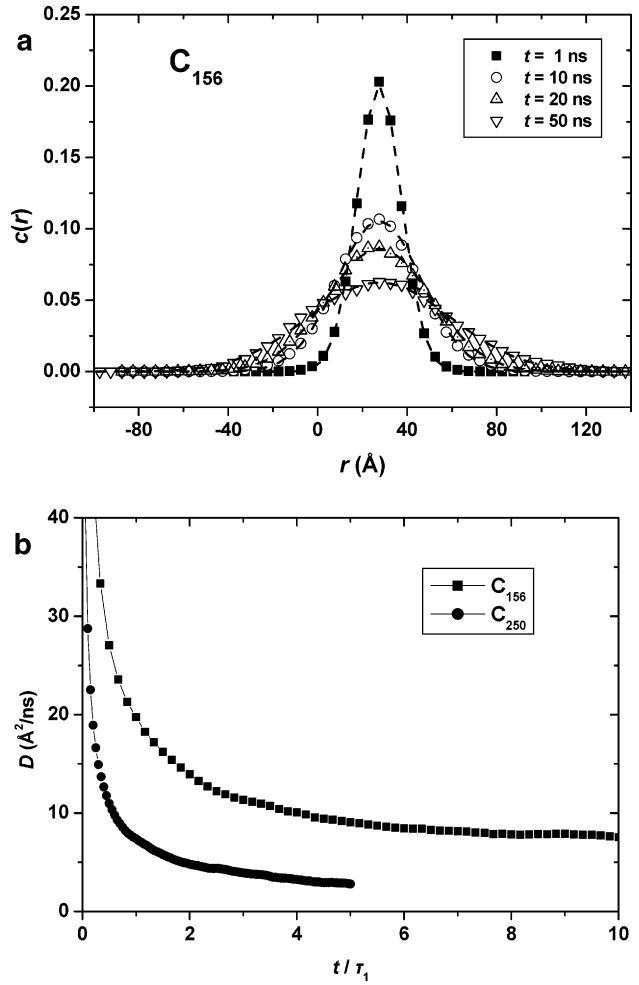

Figure 10. (a) Evolution of the normalized concentration profile of "tagged" atoms (symbols) with time in the bulk C_{156} PE melt and its fitting (lines) with the solution of the macroscopic continuum diffusion equation. (b) Time dependence of the extracted diffusion coefficients, D, as a function of chain length, N.

is commensurate with the longest relaxation time of the chains in the melt: for C_{156}, $\tau_1 \approx 6$ ns, while for C_{250}, $\tau_1 \approx 25$ ns.[51] Only after a time equal to about $5-6\tau_1$, D approaches a constant, time-invariant value representative of Fickian diffusion: this is equal to 7.5 Å^2/ns for the C_{156} PE melt and equal to 2.5 Å^2/ns for the C_{250} PE melt. These values are exactly the same with those obtained from the more sophisticated method based on the slope of the msd of segments in the terminal regime or Fickian limit,[48] which validates the new method.

New results about the transport properties of the adsorbed PE melt films simulated here are presented in Figures 11−13. Figure 11a shows the spatial distribution of carbon atoms residing initially in the part of the "large" C_{78} melt that extends up to $d = 11$ Å from the graphite phase (i.e., it covers the first two adsorption layers; see also Figure 1) at times $t = 0$, 1, 4, and 10 ns from an arbitrarily selected time origin; the corresponding concentration profiles are plotted in Figure 11b. Shown by the continuous lines in Figure 11b are the best fits to the concentration profiles with the solution of the macroscopic diffusion equation, which are seen to follow the simulation data remarkably well.

How D changes with t is shown in Figure 12. The figure demonstrates that adsorbed segments belonging to the first two adsorption layers execute a very complicated thermal motion: Starting from a very high value, their diffusion constant, initially, drops monotonically over a time period equal to 2−3 ns ($\approx 2\tau_1$) to a very low value (equal to 20 Å^2/ns); for the next 10 ns ($\approx 8\tau_1$), D remains practically constant and then rises to assume gradually the value of 32 Å^2/ns characteristic of Fickian diffusion in the bulk, unconstrained C_{78} melt. In all, it takes more than 15 ns ($\approx 12\tau_1$) for segments in the first two adsorption layers to assume bulk diffusivities. Figure 12 shows additional diffusivity data characterizing segments that initially resided in the first three adsorption layers of the confined film.

In all cases, D can never be considered as a constant. Furthermore, it is smaller for segments in the first adsorption layers than in the next. According to the data of Figure 12, D is always calculated to be smaller in the confined film than in the unconstrained bulk system. It is only for times longer than about $13\tau_1$ that adsorbed segments assume mobility features that resemble those of the corresponding bulk system. Clearly, to achieve bulklike features, the thickness d of the layer has to be larger than 17 Å. The exact value of d beyond which the transport properties of the adsorbed film approach that of the bulk, unconstrained melt can be extracted if we plot the ratio $D(t)/D(t\rightarrow\infty)$ as a function of d. This is shown in Figure 13, where $D(t)/D(t\rightarrow\infty)$ is plotted vs d for times t equal to 4, 10, and 15 ns. It is concluded that d must be at least 90 Å, i.e., $6-7R_g$, for the diffusion coefficient D in the C_{78} PE film to be equal to that in a bulk C_{78} melt.

Figures 12 and 13 suggest that the closer "tagged" segments to the attractive surface, the more inhomogeneous their diffusion is. To correlate this with the average chain size, two plots are presented in Figure 14: the first (shown by the filled symbols) is a probability-of-adsorption plot for polymer segments, as a function of the chain center-of-mass distance d from the graphite phase. [A segment is considered as adsorbed if it lies in the density-perturbed region of the film, i.e., up to 17 Å from the surface.] For chains whose center-of-mass is between 10 and 25 Å from the graphite phase, Figure 14 shows the probability-of-adsorption to decrease linearly with d, which correlates with the linear part of the $D(t)/D(t\rightarrow\infty)$-vs-$d$ plot in Figure 13. On the other hand, for chains whose center-of-mass lies beyond 40 Å from the surface, the probability of adsorption is zero. At these distances, however, the diffusion coefficient D has not still reached its bulk value (see Figure 12). This can be explained by the data of the second curve in Figure 14 (open symbols) presenting the fraction of adsorbed segments in the interfacial region as a function of region thickness d. The fraction of adsorbed segments remains high (∼30%) even in regions extending up to 40 Å ($\approx 3R_g$) from the graphite plane. This means that in a film with thickness as large as $3R_g$ a significant number of the population of diffusive carbon atoms is adsorbed, which affects the transport properties of the film as a whole, thus resulting in a slower overall segmental mobility than in the unconstrained system.

According to Figure 14, it is only for C_{78} films thicker than 100 Å ($\sim 7R_g$) that the fraction of adsorbed segments becomes small enough (∼15%) for their diffusive properties to assume bulklike features. This is verified in Figure 15 presenting the time dependence of D for carbon atoms in the large 200-chain C_{78} PE film that initially resided in a region that extends up to a distance

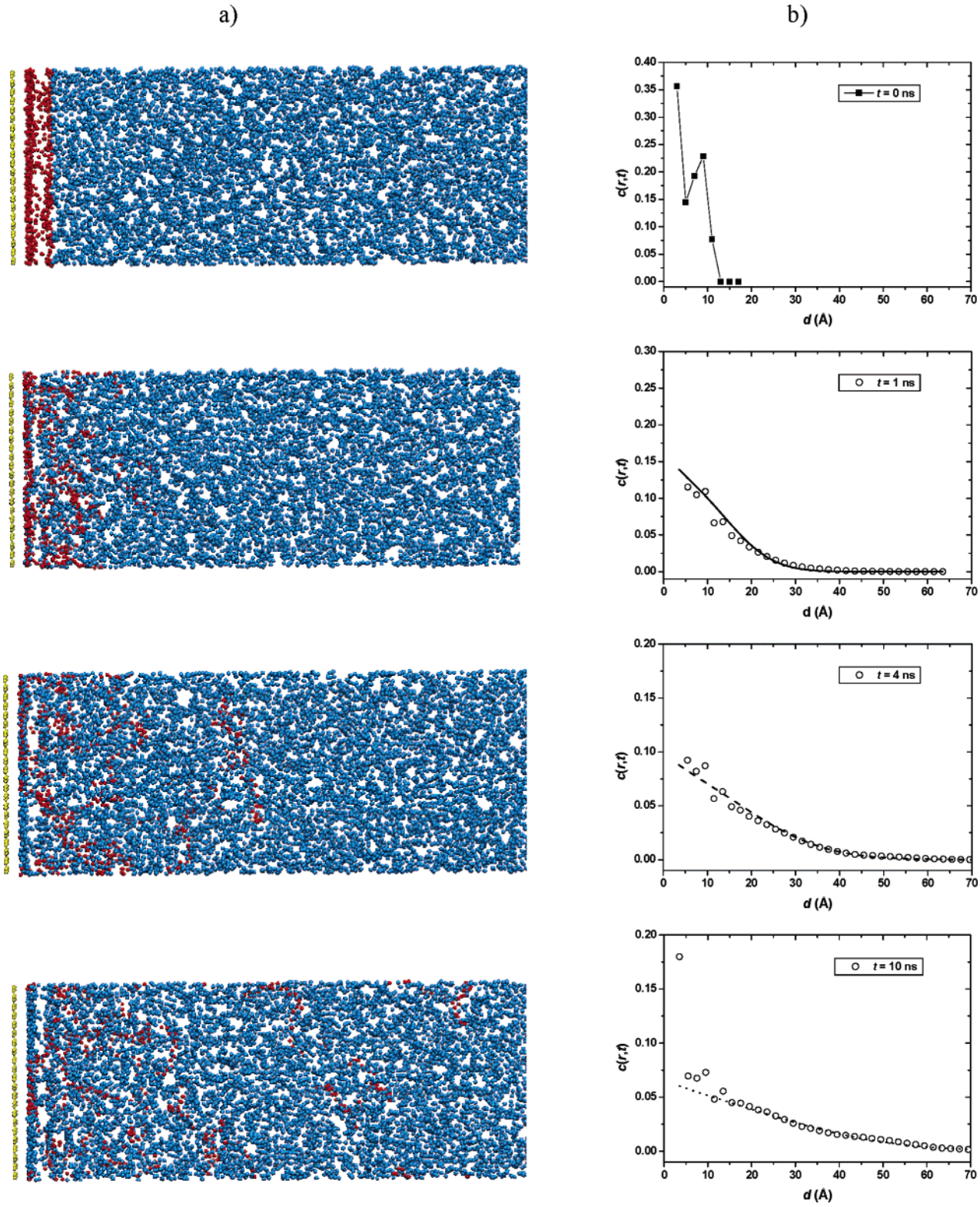

Figure 11. Schematic of segmental mobility and diffusion in the adsorbed C_{78} PE melt film. Tagged atoms (colored in red) at $t = 0$ include all adsorbed backbone carbon atoms up to a distance $d = 11$ Å from the graphite plane: (a) Spatial distribution of the population of tagged atoms at times $t = 0$, 1, 4, and 10 ns from the time origin. (b) The corresponding concentration profiles and their best fits with the solution of the macroscopic diffusion equation, eq 11.

100 Å from the graphite phase. Also shown in the figure is the curve corresponding to an unconstrained C_{78} melt (see also Figure 10). [The two curves are compared here only for times up to 15 ns since for longer time separations, segmental diffusion in the film is affected by the outer (polymer melt/vacuum) interface. In fact, for times longer than 15 ns, the enhanced atomic mobility at the free surface propagates for some distance into the bulk due to chain connectivity and affects our calculations of D in the underlying polymer, even though the density there (i.e., in the bulklike region of the film) is indistinguishable from that of the true bulk melt.] Within the statistical accuracy of the data, the two plots indeed coincide.

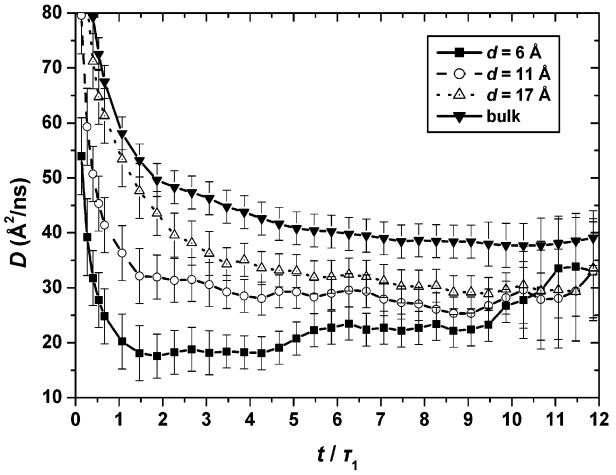

Figure 12. Diffusion coefficient, D, of adsorbed segments as a function of the thickness d of the film from the graphite plane they lie in at the time origin and how it changes with time, t. Symbols account for the time dependence of the diffusion coefficient in a bulk, unconstrained C_{78} PE melt.

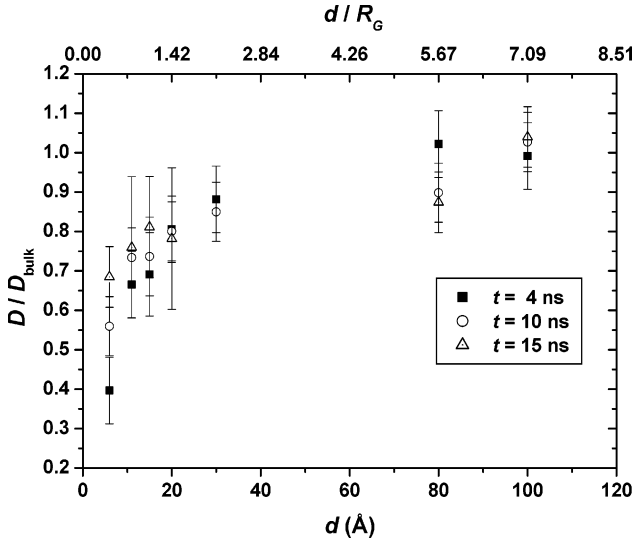

Figure 13. Dependence of the diffusion coefficient D (scaled with its value in the bulk) on the thickness d of the layer under study, at time separations equal to 4, 10, and 15 ns from the time origin, for the "large" C_{78} PE melt film.

V. Conclusions

Results have been presented for the dynamic and transport properties of linear PE melts adsorbed on a graphite phase and exposed to vacuum on the other side from detailed atomistic MD simulations in the NPT statistical ensemble at $T = 450$ K and $P = 0$ atm. The MD simulations were carried out with a multiple time step algorithm for times up to 100 ns to reliably calculate the transport properties of the adsorbed films.

Conformational relaxation at the PE melt/graphite and PE melt/vacuum interfaces was quantified through the time decay of the torsional autocorrelation function and found to be slower next to the graphite phase (at distances less than 6 Å from it) and faster at the free surface of the melt, in comparison to that in a bulk, unconstrained system of the same MW. Local mobility at the level of carbon atoms was examined in terms of the msd of segments and incoherent dynamic structure factor in the xy plane as a function of distance from the graphite surface. Consistently with the studies of conformational relaxation, these calculations showed that it is only in the first adsorption layer that carbon atoms exhibit a slower dynamics than in the bulk; in contrast, in the outer (polymer/vacuum) interface, carbon atoms move faster than bulk atoms. Short-time dynamics was also analyzed at the level of entire chains, through the definition and calculation of an apparent chain self-diffusion coefficient tensor, based on the msd of the chain centers-of-mass within a short time period. Our calculations showed that near the attractive graphite surface the chain short-time dynamics is highly anisotropic: it is slightly faster in the xy plane and much slower along the z direction.

The most significant result of our work is the evaluation of the diffusion constant D characterizing the long time motion of adsorbed segments in the direction normal to graphite, whose value in the simulated films was found to differ markedly from that in the corre-

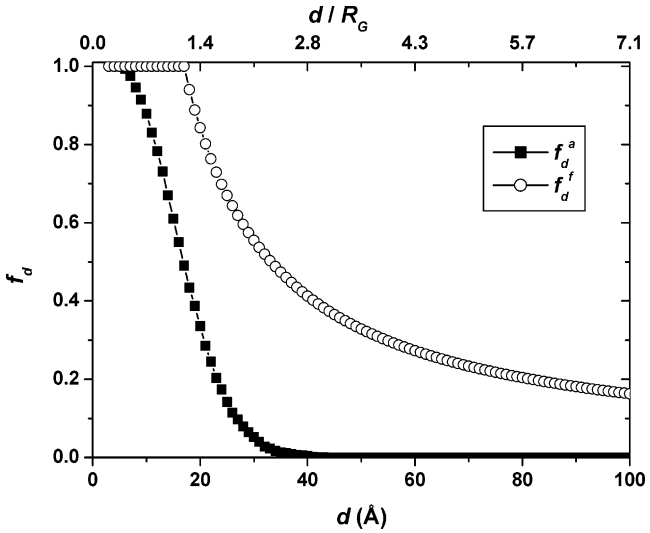

Figure 14. Fraction of adsorbed carbon atoms in the "large" C_{78} PE melt as a function of the distance from the solid surface d of the chain center-of-mass they belong to, f_d^a (filled symbols), and fraction of adsorbed atoms in the region of the adsorbed layer extending up to a distance d from the graphite phase, f_d^f (open symbols).

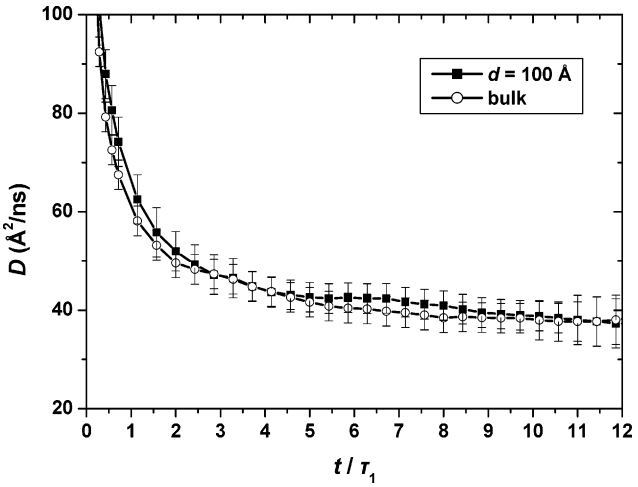

Figure 15. Dependence of the diffusion coefficient, D, of adsorbed segments on time, t, corresponding to the part of the film in the large C_{78} film that extends up to a distance d = 100 Å from the graphite phase (full symbols) and comparison against the curve $D = D(t)$ obtained from MD simulations with a bulk C_{78} melt (empty symbols).

sponding bulk, unconstrained PE systems. Results from a long MD simulation with a "large" 200-chain C_{78} PE melt showed that segmental transport in the adsorbed layer is quantitatively and qualitatively different from that in the bulk and cannot be described by the macroscopic diffusion equation with constant diffusivity, D. It can, however, be accurately described by a macroscopic diffusion equation with a time-dependent diffusion coefficient, $D(t)$. The function $D = D(t)$ was calculated here for the adsorbed 200-chain C_{78} PE melt. At short times, the rate of diffusive motion of the adsorbed segments was found to be highly complicated and anomalous, characterized by a sudden drop within a time scale commensurate with the longest (Rouse) relaxation time in the bulk, τ_1. At later times, D was found to reach a plateau value whose magnitude is significantly lower than that characterizing segmental diffusion in the bulk of the polymer at the same time instance. It was only after times at least 1 order of magnitude longer than τ_1 that segmental diffusivity in the adsorbed C_{78} PE film was observed to reach bulk features.

Local segmental diffusivities depend strongly on the thickness d of the layer next to graphite they lie at the beginning of diffusion: the closest the layer to the graphite plane (i.e., the smaller the value of d), the slower the segmental mobility. For segmental diffusion in the surface to become bulklike at all time instances, very large values of d (equal to $6-7R_g$) containing only a small number of adsorbed atoms should be considered. Experimental studies with other polymer melt/solid surface systems have proposed totally different values for such a distance, ranging from $3-4R_g$ (ref 22) to $25R_g$ (ref 20).

The present study has focused on films of unentangled PE chain systems. Future work will address the dynamics of longer, entangled PE systems on graphite and the scaling of the diffusion coefficient D with chain length. Chain mobility at the free surface of the melts will also be studied.

Acknowledgment. We are grateful to the European Community project PMILS (Polymer Modelling at Integrated time and Length Scales), Contract No. G5RD-CT-2002-00720, for financial support in the course of this work. Very fruitful discussions with Prof. Sanat Kumar are deeply acknowledged.

References and Notes

(1) Wu, S. *Polymer Interface and Adhesion*; Marcel Dekker: New York, 1982.
(2) Kinloch, A. J. *Adhesion and Adhesives: Science and Technology*; Chapman & Hall: New York, 1987.
(3) Fleer, G. J.; Cohen Stuart, M. A.; Scheutjens, J. M. H. M.; Cosgrove, T.; Vincent, B. *Polymers at Interfaces*; Chapman & Hall: London, 1993.
(4) Jones, R. A. L.; Richards, R. W. *Polymers at Surfaces and Interfaces*; Cambridge University Press: Cambridge, 1999.
(5) Tsagaropoulos, G.; Eisenberg, A. *Macromolecules* **1995**, *28*, 396, 6067.
(6) Horn, R. G.; Israelachvili, J. N. *Macromolecules* **1988**, *21*, 2836.
(7) Hu, H.; Granick, S. *Science* **1992**, *258*, 1339.
(8) Granick, S.; et al. *J. Polym. Sci., Part B: Polym. Phys.* **2003**, *41*, 2755.
(9) Daoulas, K. Ch.; Harmandaris, V. A.; Mavrantzas, V. G. *Macromolecules* **2005**, *38*, 5780.
(10) Karayiannis, N. C.; Mavrantzas, V. G.; Theodorou, D. N. *Phys. Rev. Lett.* **2002**, *88*, 105503. Karayiannis, N. C.; Giannousaki, A. E.; Mavrantzas, V. G.; Theodorou, D. N. *J. Chem. Phys.* **2002**, *117*, 5465.
(11) Steele, W. A. *Surf. Sci.* **1973**, *36*, 317.
(12) Mansfield, K. F.; Theodorou, D. N. *Macromolecules* **1989**, *22*, 3143.
(13) Mansfield, K. F.; Theodorou, D. N. *Macromolecules* **1991**, *24*, 4295.
(14) Daoulas, K. Ch.; Terzis, A. F.; Mavrantzas, V. G. *J. Chem. Phys.* **2002**, *116*, 11028.
(15) Daoulas, K. Ch.; Terzis, A. F.; Mavrantzas, V. G. *Macromolecules* **2003**, *36*, 6674.
(16) Zheng, X.; Sauer, B. B.; Van Alsten, J. G.; Schwarz, S. A.; Rafailovich, M. H.; Sokolov, J.; Rubinstein, M. *Phys. Rev. Lett.* **1995**, *74*, 407.
(17) Zheng, X.; Rafailovich, M. H.; Sokolov, J.; Strzhemechny, Y.; Schwarz, S. A.; Sauer, B. B.; Rubinstein, M. *Phys. Rev. Lett.* **1997**, *79*, 241.
(18) Pu, Y.; Rafailovich, M. H.; Sokolov, J.; Gersappe, D.; Peterson, T.; Wu, W.-L.; Schwarz, S. A. *Phys. Rev. Lett.* **2001**, *87*, 206101.
(19) Hu, X.; Zhang, W.; Si, M.; Gelfer, M.; Hsiao, B.; Rafailovich, M.; Sokolov, J.; Zaitsev, V.; Schwarz, S. *Macromolecules* **2003**, *36*, 823.
(20) Frank, B.; Cast, A. P.; Rusell, T. P.; Brown, H. R.; Hawker, C. *Macromolecules* **1996**, *29*, 6531.
(21) Hall, D.; Miller, R.; Torkelson, J. *J. Polym. Sci., Part B* **1997**, *35*, 2795.
(22) Lin, E.; Wu, W.; Satija, S. *Macromolecules* **1997**, *30*, 7224.
(23) Fuhrmann, D.; Criswell, L.; Mo, H.; Volkmann, U. G.; Herwig, K. W.; Taub, H.; Hansen, F. Y. *Physica B* **2000**, *276*, 345.
(24) Lin, W.-Y.; Blum, F. D. *Macromolecules* **1998**, *31*, 4135.
(25) Rivilon, S.; Auroy, P.; Deloche, B. *Phys. Rev. Lett.* **2000**, *84*, 499.
(26) Doi, M.; Edwards, S. F. *The Theory of Polymer Dynamics*; Clarendon Press: Oxford, 1986.
(27) Bitsanis, I. A.; Hatziioannou, G. *J. Chem. Phys.* **1990**, *92*, 3827.
(28) Bitsanis, I. A.; Brinke, G. *J. Chem. Phys.* **1993**, *99*, 3100.
(29) Smith, G. D.; Yoon, D. Y.; Jaffe, R. L. *Macromolecules* **1992**, *25*, 7011.
(30) Winkler, R. G.; Matsuda, T.; Yoon, D. Y. *J. Chem. Phys.* **1993**, *98*, 731.
(31) Matsuda, T.; Smith, G. D.; Winkler, R. G.; Yoon, D. Y. *Macromolecules* **1995**, *28*, 165.
(32) Yoon, D. Y.; Vacatello, M.; Smith, G. D. In *Monte Carlo and Molecular Dynamics Simulations in Polymer Science*; Binder, K., Ed.; Oxford University Press: New York, 1995.
(33) Aoyagi, T.; Takimoto, J.; Doi, M. *J. Chem. Phys.* **2001**, *115*, 552.
(34) Wang, Y.; Rajagopalan, R. *J. Chem. Phys.* **1996**, *105*, 696.
(35) Lai, P. Y. *Phys. Rev. E* **1994**, *49*, 5420.
(36) Milchev, A.; Binder, K. *J. Chem. Phys.* **2001**, *114*, 8610.
(37) Mischler, C.; Baschnagel, J.; Dasgupta, S.; Binder, K. *Polymer* **2002**, *43*, 467.
(38) Varnik, F.; Baschnagel, J.; Binder, K. *Eur. Phys. J. E* **2002**, *8*, 175.
(39) Ponomarev, A. L.; Sewell, T. D.; Durning, C. J. *Macromolecules* **2000**, *33*, 2662.
(40) Smith, G. D.; Bedrov, D.; Borodin, O. *Phys. Rev. Lett.* **2003**, *90*, 226103.
(41) Borodin, O.; Smith, G. D.; Bandyopadhyaya, R.; Byutner, O. *Macromolecules* **2003**, *36*, 7873.
(42) Salvatore, L.; Delle Site, L.; Kremer, K. Manuscript in preparation.
(43) Van der Ploeg, P.; Berendsen, H. J. *J. Chem. Phys.* **1982**, *76*, 3271.
(44) Toxvaerd, S. *J. Chem. Phys.* **1997**, *107*, 5197.
(45) Martin, M. G.; Siepmann, J. I. *J. Phys. Chem. B* **1998**, *102*, 2569.
(46) Trokhymchuk, A.; Alejandre, J. *J. Chem. Phys.* **1999**, *111*, 8510.
(47) van Megen, W.; Mortensen, T. C.; Williams, R. C.; Müller, J. *Phys. Rev. E* **1998**, *58*, 6073.
(48) Harmandaris, V. A.; Mavrantzas, V. G. Molecular Dynamics Simulation of Polymers. In *Simulation Methods for Modeling Polymers*; Theodorou, D. N., Kotelyanskii, M. J., Eds.; Marcel Dekker: New York, 2004.
(49) Mavrantzas, V. G. Monte Carlo Simulation of Chain Molecules. In *Handbook of Materials Modeling. Volume I: Methods and Models*; Yip, S., Ed.; Springer: Dordrecht, The Netherlands, 2005; pp 1−15.
(50) Theodorou, D. N. Variable-connectivity Monte Carlo algorithms for the atomistic simulation of long-chain polymer systems. In Nielaba, P., Mareschal, M., Ciccotti, G., Eds.;

Bridging Time Scales: Molecular Simulations for the Next Decade; Springer-Verlag: Berlin, 2002.
(51) Harmandaris, V. A.; Mavrantzas, V. G.; Theodorou, D. N. *Macromolecules* **1998**, *31*, 7934; **2003**, *36*, 1376.
(52) Ferrero, M.; Chiovetta, M. *Polym. Eng. Sci.* **1987**, *27*, 1436, 1447.
(53) Hutchiston, R.; Chen, C.; Ray, W. *J. Appl. Polym. Sci.* **1992**, *44*, 1389.
(54) Estenoz, D.; Chiovetta, M. *J. Appl. Polym. Sci.* **2001**, *85*, 285.
(55) Laso, M.; Jimeno, N.; Muller, M. *Polym. React. Eng.* **2003**, *11*, 1.
(56) McQuarie, D. A. *Statistical Mechanics*; Harper and Row: New York, 1976.
(57) Dassios, G.; Kyriaki, F. *Partial Differential Equations* (in Greek); Patras University Press: Patras, 1994.
(58) Press, W. H.; Teukovski, S. A.; Vettering, W. T.; Flannery, B. P. *Numerical Recipes*; Cambridge University Press: Cambridge, 1996.
(59) Crank, J. *The Mathematics of Diffusion*; Oxford University Press: Oxford, 1975.

MA050177J